Dentomaxillofacial Radiology (2015) 44, 20140157

birpublications.org/dmfr

RESEARCH ARTICLE

Evaluation of intensity of artefacts in CBCT by radio-opacity of composite simulation models of implants *in vitro*

[1,2]N Kuusisto, [2]P K Vallittu, [2]L V J Lassila and [1,3]S Huumonen

[1]*Department of Oral Pathology and Radiology, Institute of Dentistry, University of Turku, Turku, Finland;* [2]*Department of Biomaterials Science and Turku Clinical Biomaterials Centre—TCBC, Institute of Dentistry and BioCity, University of Turku, Turku, Finland;* [3]*Department of Diagnostic Imaging, Turku University Hospital, Turku, Finland*

Objectives: The aim was to compare the intensity of artefacts in CBCT images caused by different percentages of radio-opacifying material in composite simulation models of implants. Titanium and zirconia models of implants were used as a reference for the evaluation of the intensity of artefacts.
Methods: Seven different percentages of radio-opacifying $BaAlSiO_2$ fillers were added to composite resin to fabricate seven step wedges and simulation models of implants. Titanium and zirconia simulation models of implants were also fabricated. Aluminium step wedge was used as a reference for the measurement of grey values in intraoral radiographs. Step wedges were exposed with a Planmeca Intra X-ray machine (Planmeca Oy, Helsinki, Finland). All composite, titanium and zirconia simulation models of implants were exposed with a SCANORA® 3D dental X-ray machine (Soredex, Tuusula, Finland). Images and grey values were analysed with ImageJ software (National Institutes of Health, Bethesda, MD). To demonstrate possible artefacts between all the simulation models of implants, the images were also visually compared with each other using ImageJ software.
Results: Artefacts were clearly present in CBCT images caused by titanium and zirconia and when the composite material consisted at least 20% $BaAlSiO_2$. The intensity of artefacts increased when the radio-opacity of the composite material increased.
Conclusions: Materials containing less radio-opacity produce less pronounced artefacts. The cut-off point for artefacts is at 20% radio-opaque filling material in composite material.
Dentomaxillofacial Radiology (2015) **44**, 20140157. doi: 10.1259/dmfr.20140157

Cite this article as: Kuusisto N, Vallittu PK, Lassila LVJ, Huumonen S. Evaluation of intensity of artefacts in CBCT by radio-opacity of composite simulation models of implants *in vitro*. *Dentomaxillofac Radiol* 2015; **44**: 20140157.

Keywords: artifact; cone beam CT; radio-opacity; composite-based implant model

Introduction

CBCT is increasingly used in dentistry and maxillofacial imaging in diagnosis, treatment planning and follow-up.[1–5] With CBCT, several artefacts may occur related to the technique itself and the object being examined. Artefact is any distortion or error in the image that is unrelated to the object being examined. The most common artefacts with CBCT caused by dense materials are beam-hardening artefacts, extinction artefacts and exponential edge gradient effect artefacts. Beam-hardening artefacts appear as dark streaks adjacent to areas of high density. The artefact occurs because the high density of the object absorbs the lower energy photons while the higher energy photons pass through to the detectors which results in the beam becoming harder, that is, contains more wavelengths of higher energy. Extinction artefacts are also caused by highly absorbing material. Basically, extinction artefacts are caused because of the rise of the absorption of mean energy.[6] Exponential edge gradient effect artefacts occur when the object is angular and much more radio-opaque than the

Correspondence to: Dr Sisko Huumonen. E-mail: sisko.huumonen@utu.fi
Received 18 May 2014; revised 27 September 2014; accepted 2 October 2014

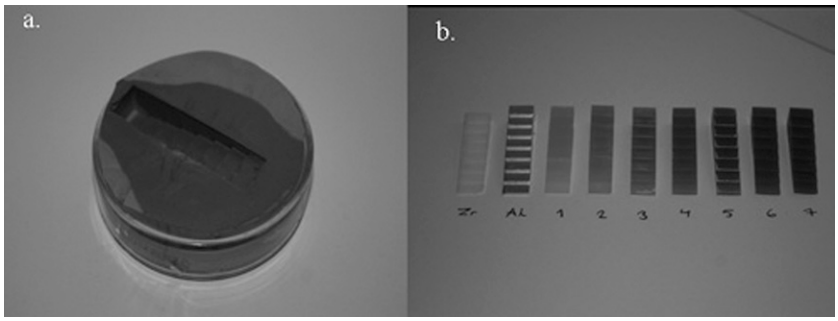

Figure 1 (a) The mould for step wedges, diameter 50 mm, height 10 mm; (b) zirconia, aluminium and the composite step wedges.

surrounding structures. The exponential edge gradient effect artefacts are seen as lines towards straight edges in the projection direction.[6] The intensity of beam-hardening artefacts was assessed in this study.

When CBCT is used in regions containing dense objects, such as metal implants, artefacts may reduce the diagnostic value in close proximity to implants.[6,7] Knowledge of the presence, shape, intensity and typical regions of artefacts will help in planning and interpreting CBCT examinations. The radio-opacity of material is dependent on the density of the material, that is, on the atomic number of the elements used in the components of the dental restorations or implants.[8,9]

In oral and cranial implantology, emphasis has been put on the development of non-metallic implants, such as implants made of composite materials.[10–14] Compared with metal implants, composite implants, especially fibre-reinforced composite (FRC) implants, are low weight and provide possibilities to tailor mechanical properties equal to those of the bone.[15–17] In addition, composite and FRC implants can be detected with CT and MRI.[14]

CBCT examinations might be considered in the follow-up of implants in the dental and maxillofacial region if artefacts caused by the implants could be reduced or even avoided. Therefore, the purpose of this study was to compare the intensity of artefacts in CBCT images caused by established materials such as titanium and zirconia and seven different percentages of radio-opacifying material in composite simulation models of implants. In addition, the purpose was to find out how much the grey values near composite implants differ from the metal implants and what composite implants cause artefacts.

Methods and materials

Preparation of the step wedge mould

The mould for composite step wedges was made of Putty Soft polyvinyl siloxane (Coltene/Whaledent, Altstätten, Switzerland). A standard measuring scoop portion of Putty Soft Base and Putty Soft Catalyst was mixed to form a smooth mixture. The mixture was applied to a round glass bowl (Figure 1a). An aluminium step wedge was used to make a model for step wedges. The impression material Affinis® Precious (Coltene/Whaledent) was spread on the aluminium step wedge. This made it possible to copy the shape of the step wedge. The aluminium step wedge was then pressed so deep into the Putty mixture that only the bottom of the step wedge was visible. The mixture was allowed to harden for 3 min (Figure 1a).

Preparation of the composite step wedges

Seven different kinds of composite step wedges were prepared (Figures 1b and 2). Thermally polymerized resin composite [bisphenal A glycidyl methacrylate (Bis-GMA) (70%) + tetraethylene glycol dimethacrylate (TEGDMA) (30%)], 1% benzoyl peroxide (BPO), silicon dioxide (SiO_2; 2%) and $BaAlSiO_2$ were used for the preparation. All step wedges contained different percentages of SiO_2 and $BaAlSiO_2$. The percentages of fillers are shown in Table 1. Fillers were added gradually to the resin and mixed for 30 s in a speed mixer (SpeedMixer™ DAC 150 FVZ; Hauschild, Germany) operating at 1700 rpm. Mixing was repeated three times until the mixture was dense and easy to handle. The composite mixture was applied into the step wedge mould and pressed with a sheet glass so that the bottom of the step wedge became flat. The composite mixture was polymerized for 15 min in pressure curing unit (Ivomat IP12, Ivoclar ag.; Schaan, Liechtenstein) at 100 °C in 200 kPa.

Preparation of the simulation models of implants

Seven different radio-opacity levels of composite cylinders were prepared to simulate composite implants. The percentage compositions of SiO_2 and $BaAlSiO_2$ were the same as those of the step wedges (Table 1). The mould for implant simulation models was made of Lab Putty (Coltene/Whaledent). A standard measuring scoop portion of Lab Putty and Lab Putty Catalyst was mixed to form a smooth mixture. A titanium control cylinder (20 mm in height, 3 mm in diameter) was put into the Putty. The Putty mixture was allowed to harden

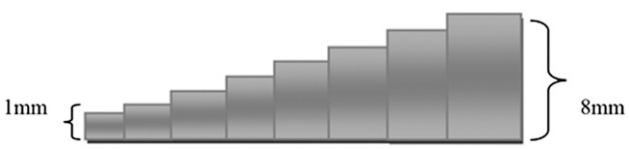

Figure 2 Dimensions of the step wedges that were used for intraoral radiography and to study how materials correspond to each other.

Table 1 The percentage compositions of $BaAlSiO_2$ and silicon dioxide (SiO_2) in the composite step wedges and composite simulation models of implants

Composite step wedge/implant	*First group*	*Second group*	*Third group*	*Fourth group*	*Fifth group*	*Sixth group*	*Seventh group*
$BaAlSiO_2$ (weight%)	68	64	57	47	32	20	0
SiO_2 (weight%)	0	6	14	25	38	49	74

for 5 min. Composite mixture was polymerized for 15 min in pressure curing unit (Ivomat IP12, Ivoclar ag.) at 100 °C, in 200 kPa. Composite simulation models of implants were honed to the same dimension as the titanium cylinder. Owing to increasing clinical use of zirconia as dental implant and restorative material, additional measurement was made with a zirconia cylinder, which corresponded to the size of the titanium and composite implant simulation models.

Radiographic imaging

Composite step wedges were exposed with the aluminium step wedge using a Planmeca Intra X-ray machine (Planmeca Oy, Helsinki, Finland) operating at 63 kV and 5–8 mA (Figure 3). The intraoral sensor was a solid-state sensor Planmeca Dixi (Planmeca Oy). Focus–sensor distance was 24.5 cm, and exposure time was between 0.08 and 0.20 s.

Composite, titanium and zirconia simulation models of implants were exposed in groups of three and separately in a Teflon® block using a SCANORA® 3D dental X-ray machine (Soredex, Tuusula, Finland) operating at 90 kV and 12 mA. The exposure time was 7.43 s. Figure 4 shows how the implants were placed in the Teflon block. The Teflon block was in the same position during the exposures.

Image analysis

Intraoral radiographs were saved as JPEG images (8-bit). The grey values of the composite step wedges were analysed with ImageJ software (Figure 3) which is an image processing program developed at the National Institutes of Health (Bethesda, MD). Each step of the composite step wedges was compared with aluminium steps in ImageJ as a pixel point analysis (Figure 3). For the results, one average grey value of each step was used.

CBCT slices were saved as TIFF (16-bit) radiographs. 1-mm thick axial CBCT slices were analysed with ImageJ software. The grey values of the artefacts were measured from the line (ImageJ) through the implants (Figure 4). The histograms of the simulation models of implants of CBCT slices were created from this line with ImageJ software (Figure 5).

Results

Intraoral radiographs

Comparisons of the step wedges are shown in Figures 6 and 7, in which the intensity of the artefacts in CBCT images and the corresponding materials that could cause similar artefacts in CBCT images can be estimated. Composite step wedges were compared with aluminium steps (Figure 3), and based on these grey values, a diagram was formed in which different materials of this study can be compared with aluminium (Figures 6 and 7).

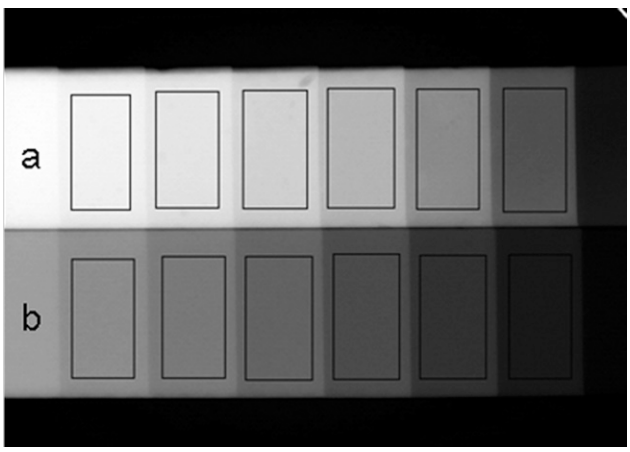

Figure 3 An intraoral radiograph. Squares show the areas where grey values were measured. For the results, a mean grey value of the square area of the steps was used. (a) The composite step wedge. (b) The aluminium step wedge.

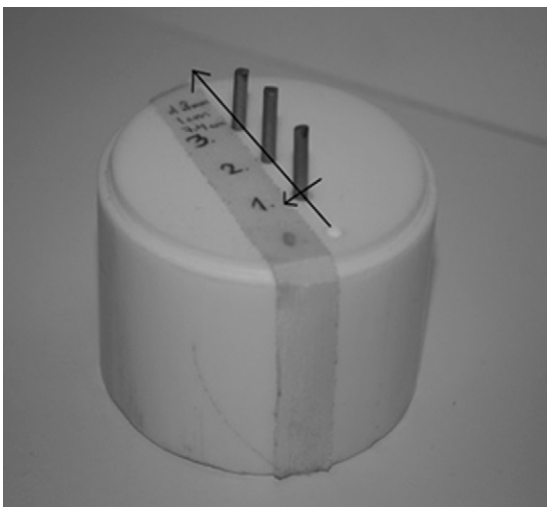

Figure 4 The Teflon® block used in CBCT examinations. The black line shows the direction of the histogram made of the axial CBCT slice using ImageJ software (National Institutes of Health, Bethesda, MD). The grey values of the artefacts were measured from this line. The block has a diameter of 72 mm, height of 46 mm and slot diameter of 3.5 mm. Distance between the holes is 10 mm.

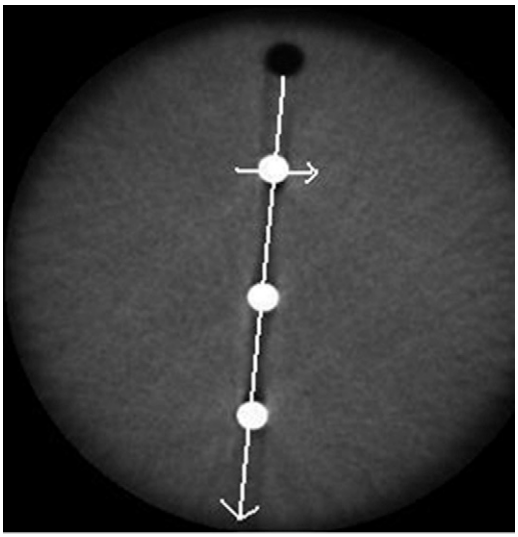

Figure 5 An axial CBCT slice of Teflon® block with three implant simulation models (white) used in the study. The white line shows where the histogram was taken.

CBCT images

Composite titanium and zirconia simulation models of implants were compared in axial CBCT slices. Intensity and location of artefacts can be compared in axial CBCT slices (Figure 8). All the images had the same exposure values, and analyses were performed on the same part of the composite and metal simulation models of implants. Next to the CBCT slices plot profile histograms are shown (from ImageJ) in which the numeric values of grey level of simulation models of the implants and artefacts between the implants (Figure 8) can be followed. Plot profile histograms give visual support to the grey value analysis.

Results of intraoral radiographs and CBCT images

Intraoral images showed that Implant 1 composite model (Model 1) corresponded approximately to titanium in grey values (Figure 6). The grey values of composite Models 1 and 2 were close to each other (Figure 7). No differences were found between these models in causing artefacts in CBCT images. The composite Models 1 and 2 caused almost as intense artefacts as titanium in CBCT images.

Composite models of Implants 3 and 4 (Models 3 and 4) corresponded approximately to each other in grey values (Figure 7). The estimated grey value of enamel was close to the composite models of Implants 3 and 4 (Figure 6). These composite models of implants caused less intense artefacts than did titanium and composite models of Implants 1 and 2. Composite model of Implant 5 (Model 5) had a lower grey value than did Models 3 and 4 (Figure 7) and caused less intense artefacts than Models 3 and 4.

Composite Model 6 corresponded approximately to aluminium (Figure 7). It caused less intense artefacts than did Model 5. Composite Model 7 did not contain the radio-opacifying ($BaAlSiO_2$) filling material, and the grey values were lower than for any other implant model. Composite Model 7 did not cause artefacts.

Titanium and zirconia simulation models of implants caused intense artefacts in CBCT images, especially between the implants (Figure 8a). The plot profile diagram next to the CBCT image (Figure 8a) shows that compared with composite Implants 4, 5 and 6 (Figure 8c), grey values are lower between the titanium implant models because of the more intense artefacts between the titanium models.

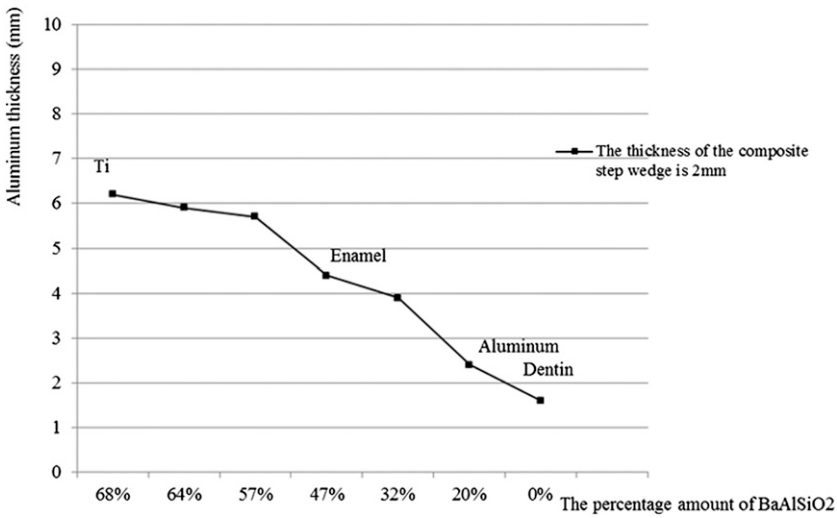

Figure 6 The results of intraoral radiographs. Grey values of aluminium step wedge (mm) on *y*-axis and 2-mm thick composite steps on *x*-axis. The line shows the grey values of corresponding thickness of the aluminium step (*y*-axis) when composite steps are 2-mm thick. The percentage amounts of $BaAlSiO_2$ (*x*-axis) describe the amount of radio-opacifying material of the composite step wedges (Table 1). Estimated grey values of corresponding thicknesses of titanium, enamel and dentin (modified from Whaites[9]) are also added. Composite implant Model 1 corresponds approximately to titanium. Composite Model 4 corresponds to enamel and composite Model 6 corresponds approximately to aluminium.

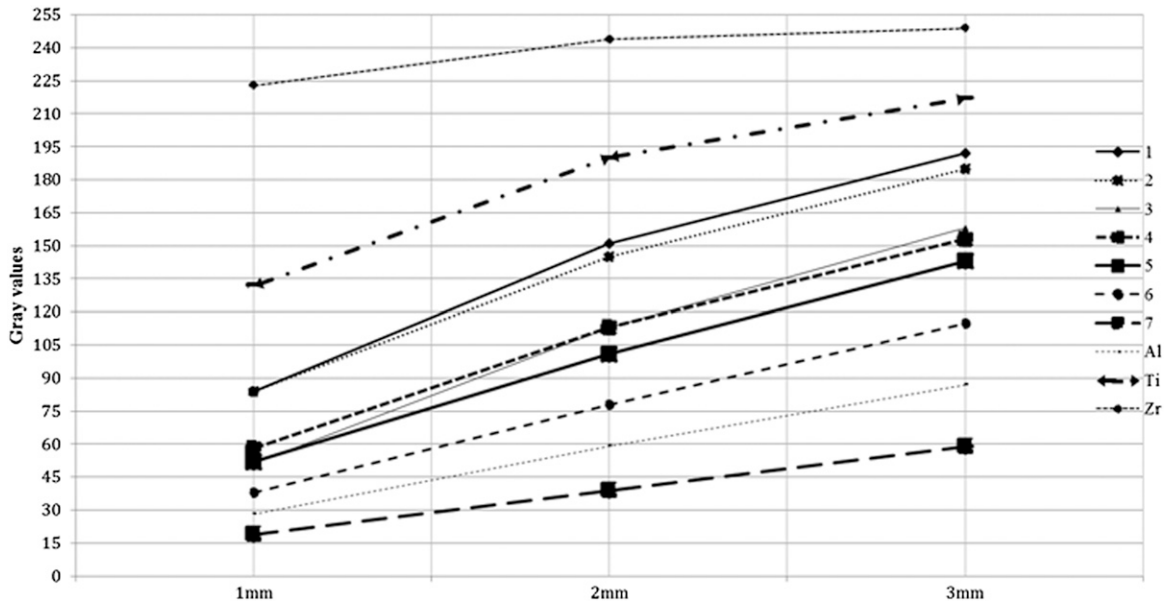

Figure 7 Grey values of the step wedges. All the step wedges (composite step wedges 1–7, titanium (Ti), aluminium (Al) and zirconia (Zr) step wedges) in the same diagram show grey values on *y*-axis. The thickness of the step wedges is shown on the *x*-axis. Grey values are close to each other between the composite Models 1 and 2 as well as 3 and 4. Grey values of the Model 7 are the lowest. The grey value of zirconia saturates at the top; its linear growth ends at 2-mm thickness.

Discussion

Except for composite Model 7, which did not have radio-opacifying material, all the composite implant models caused artefacts in the present study. Even the smallest amount of $BaAlSiO_2$ (20%) caused slight artefacts. The intensity of artefacts increased as the percentage of radio-opacifying material increased, and 68% of radio-opacifying material caused almost as intense artefacts as titanium. Zirconia caused high-intensity artefacts that deteriorated the CBCT image. When several implant simulation models were placed in a row, the intensity of artefacts between the simulation models was multifold. The use of <20% of $BaAlSiO_2$ could have given more information about the type and severity of artefacts. To our knowledge, this is the first study to investigate the effect of radio-opacity of composite material widely used in dentistry. In addition to dentistry, the suitability of composite materials in maxillofacial implants has recently been studied.[11,13,18,19]

Post-operative radiographic controls of all kinds of implants add valuable information, for example, for evaluation of possible bone resorption around the implant caused by inflammation or instability. CT or CBCT is often the preferred examination. Therefore, development of composition of implants that do not cause disturbing artefacts might be interesting.

This study focused on the composite models and their consistency of $BaAlSiO_2$ that causes actual radio-opacity. SiO_2 was used in composite models as a filling material. Composite models were prepared using thermally polymerized resin composite [Bis-GMA (70%) + TEGDMA (30%)] and 1% BPO that does not have any radio-opacity. Methacrylate monomers such as Bis-GMA and TEGDMA are widely used in dental resin-based materials as well as in FRC implant designs used in cranial and maxillofacial area, and were thus considered appropriate for use in this study as well.[19–21] In general, dental resin-based materials are required to be biocompatible, adhesive, appropriate in terms of mechanical properties,[21–23] radio-opaque and antibacterial; in addition, polymerization shrinkage and water solubility should be as small as possible.[24–26] In cranial and maxillofacial areas, resin-based composite implants are also supposed to attach to the bone.[15,18,27]

Radio-opacity in dental resin-based materials is obtained with radio-opacifying fillers such as BaO, $BaSO_4$, TiO_2, SrO and ZrO_2.[28–30] The radio-opacity is basically dependent on the atomic number of the material. As the atomic number increases, the number of bound inner-shell electrons also increases. The approximate difference for X-ray absorption for soft tissue is 7; for bone is 12; for aluminium is 13 and for dental enamel is 16 (modified from Whaites[9]).

This study examined artefacts affected by radio-opacity of composite and metal simulation implants using SCANORA 3D CBCT device. It seems that there are differences between CBCT machines in producing artefacts.[31–34] Exposure conditions can have a great role in producing artefacts by influencing the energy of the photons; some studies have recommended imaging techniques with high kilovoltage peak to decrease hardening of the beams.[31,35] Other factors that can have a role in beam hardening include the amount of rotation of the machine, the configuration of the X-ray beam and the type of the algorithm used for data processing.[36–38] In the clinic, it has

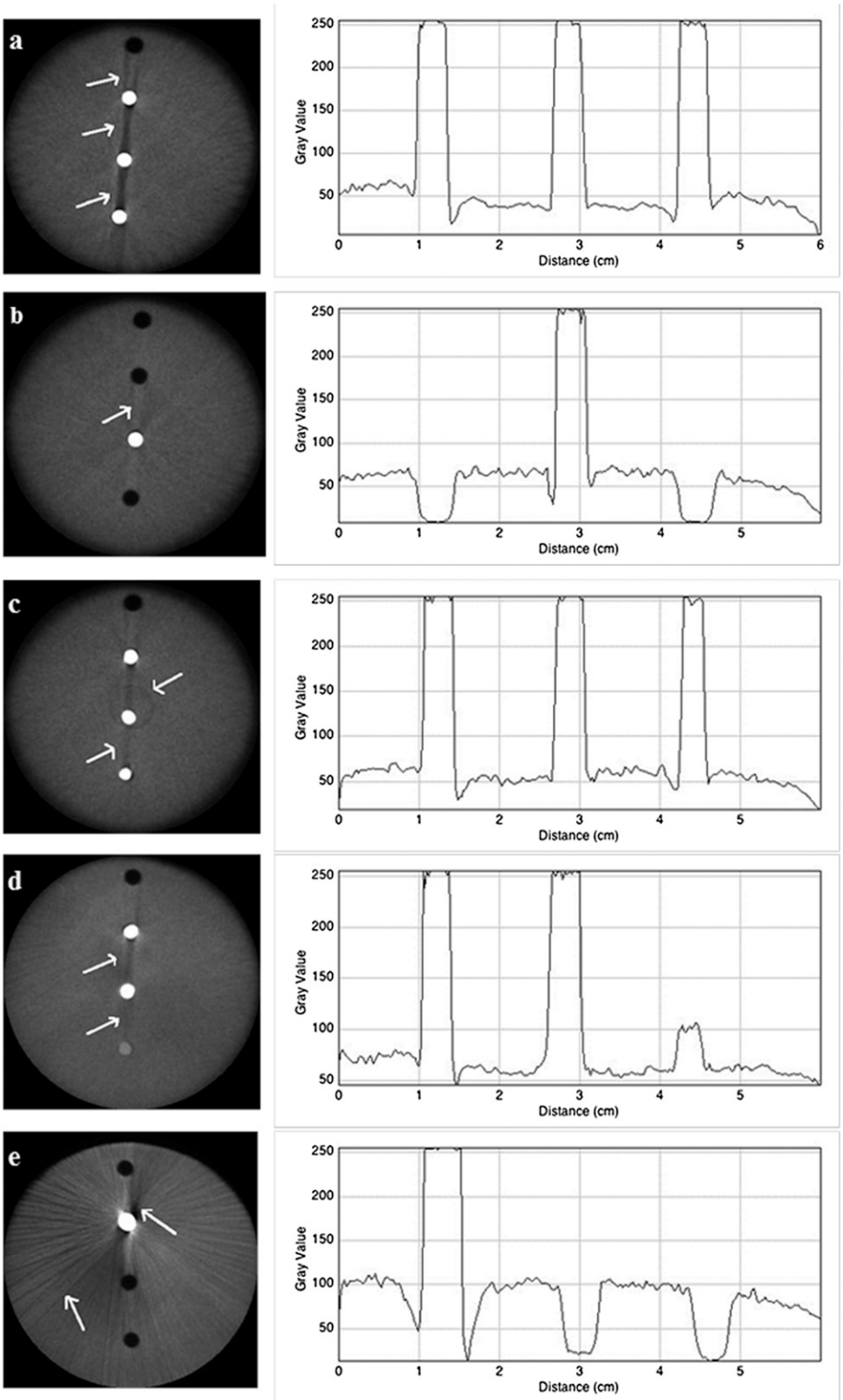

Figure 8 CBCT slices showing different simulation models of implants and comparisons of artefacts. Next to them are plot profile histograms that were compared with each other regarding the artefacts. These histograms visualize the differences of artefacts. (a) Three titanium simulation models of implants. Artefacts (arrows) are clearly seen between the implants. (b) One titanium simulation model of implant. Artefacts are lighter than those caused by the three titanium implants (a), and they are only seen near the implant. (c) Composite simulation models of implants 4, 5 and 6. Artefacts are seen, but they are not as intense as those caused by titanium. (d) Composite simulation models of implants 4, 5 and 7. Artefacts are only clearly seen between Implants 4 and 5 (upper arrow). Model 7 does not cause artefacts (lower arrow). (e) Zirconia implant. Artefacts are intense. (b, c, e) Examples of artefacts that were visually estimated are indicated by arrows.

been suggested to decrease the field of view, change the position of the patient's head or separate dental arches in order to avoid scanning the areas susceptible to beam hardening.[39] It has also been stated that the CBCT devices should be optimized by enabling exposure factors that are appropriate for artefact reduction and other image quality parameters, finding a balance with the radiation dose.[34]

Measurements of radiographs in this study were carried out using numeric values of grey level that represented the intensity that artefacts caused at different distances from the objects studied. Previous reports have also measured grey values around titanium.[31,34] The choice of the points for measurements was carried out manually, which can affect the results. On the other hand, the histograms showed that the grey values were similar in regions that were not affected by artefacts. Therefore, the comparisons of measurements can be considered reliable.

In line with earlier reports, both metallic-simulating models of implants, titanium and zirconia, caused high-intensity artefacts. Investigation of imaging of artefacts with NewTom® 9000 CBCT device (Quantitive Radiology, Verona, Italy) and Philips MX 8000 multidetector medical CT (Koninklijke Philips Electronics, N.V. Eindhoven, Netherlands) showed that artefacts were frequently observed in axial slices.[38] Artefacts have been shown to be always present near titanium implants.[31,40] In these studies, the position of implant did not affect the artefacts. However, the grey value reduction decreased with increasing distance from the implant surface, which is in agreement with the results of the present study.

In this study, Teflon was used as a background material for all simulation models of implants. Teflon is a homogeneous material and does not cause artefacts. In Teflon, it was possible to drill places for simulation models of implants. The round shape of the Teflon block and the places for simulation models of implants in a straight row was not the most ideal set-up. Thus, the distances of the incoming X-rays were not the same for every implant simulation model in the CBCT examination.

It was previously reported that artefacts were less pronounced in those *in vitro* studies where the tested materials were placed in human teeth and jaws as compared with homogenous plastic material. The density response in CBCT examinations depends on the total mass inside and outside the area of interest.[41] Less pronounced artefacts could be explained by the presence of complex anatomical structures, such as bone, teeth and enamel, instead of homogenous background as in this study. Anatomical structures seem to be able to "hide" the artefacts.

Based on the results of this study, it can be concluded that composite materials containing less radio-opacity give less pronounced artefacts in CBCT examinations. The cut-off point of artefacts is at 20% radio-opaque filling material in composite implants. If the proportion of radio-opaque filling material in composite implants exceeds 68%, artefacts as intense as with titanium implants can be expected. When several simulation models of implants are placed side by side, the intensity of artefacts becomes multifold.

References

1. Mozzo P, Procacci C, Tacconi A, Martini PT, Andreis IA. A new volumetric CT machine for dental imaging based on the cone-beam technique: preliminary results. *Eur Radiol* 1998; **8**: 1558–64.
2. Arai Y, Tammisalo E, Iwai K, Hashimoto K, Shinoda K. Development of a compact tomographic apparatus for dental use. *Dentomaxillofac Radiol* 1999; **28**: 245–8.
3. Linsenmaier U, Rock C, Euler E, Wirth S, Brandl R, Kotsianos D, et al. Three-dimensional CT with a modified C-arm image intensifier: feasibility. *Radiology* 2002; **224**: 286–92.
4. Araki K, Maki K, Seki K, Sakamaki K, Harata Y, Sakaino R, et al. Characteristics of a newly developed dentomaxillofacial X-ray cone beam CT scanner (CB MercuRay): system configuration and physical properties. *Dentomaxillofac Radiol* 2004; **33**: 51–9.
5. Scarfe WC, Farman AG. What is cone beam CT and how does it work? *Dent Clin North Am* 2008; **52**: 707–30. doi: 10.1016/j.cden.2008.05.005
6. Schulze R, Heil U, Gross D, Bruellmann DD, Dranischnikow E, Schwanecke U, et al. Artifacts in CBCT: a review. *Dentomaxillofac Radiol* 2011; **40**: 265–73. doi: 10.1259/dmfr/30642039
7. Suomalainen A. Thesis. Cone beam computed tomography in oral radiology. 2010. Available from: http://urn.fi/URN
8. Watts DC. Radiopacity vs. composition of some barium and strontium glass composites. *J Dent* 1987; **15**: 38–43.
9. Whaites E. The production, properties and interactions of X-rays. In: Whaites E, ed. *Essentials of dental radiography and radiology*. London, UK: Elsevier; 2007. pp 21–2.
10. Ballo AM, Kokkari AK, Meretoja VV, Lassila LL, Vallittu PK, Narhi TO. Osteoblast proliferation and maturation on bioactive fiber-reinforced composite. *J Mater Sci Mater Med* 2008; **19**: 3169–77.
11. Aitasalo K, Piitulainen JM, Rekola J, Vallittu PK. Craniofacial bone reconstruction with bioactive fibre composite implant. *Head Neck* 2014; **36**: 722–8. doi: 10.1002/hed.23370
12. Abdulmajeed AA, Närhi TO, Vallittu PK, Lassila LV. The effect of high fiber fraction on some mechanical properties of unidirectional glass fiber-reinforced composite. *Dent Mater* 2011; **27**: 313–21. doi: 10.1016/j.dental.2010.11.007
13. Peltola M, Vallittu PK, Vuorinen V, Aho A, Puntala A, Aitasalo K. Novel composite implant in craniofacial bone reconstruction. *Eur Arch Otorhinolaryngol* 2012; **269**: 623–8. doi: 10.1007/s00405-011-1607-x
14. Aous Abduljameed Thesis. Unidirectional fiber-reinforced composite as an oral implant abutment material. 2013: 10–67. Available from: http://www.doria.fi/handle/10024/93810
15. Vallittu PK. A review of fiber-reinforced denture base resins. *J Prostodont* 1996; **5**: 270–6.
16. Vallittu PK. Flexural properties of acrylic resin polymers reinforced with unidirectional and woven glass fibers. *J Prosthet Dent* 1999; **81**: 318–26.
17. Tuusa S, Peltola M, Tirri T, Lassila L, Vallittu PK. A review of two animal studies dealing with biological responses to glass-fibre-reinforced composite implants in critical size calvarial bone defects in rabbits. *Key Eng Mater* 2007; **20**: 471–4.
18. Ngaga S. Thesis. Development of porous glass-fiber reinforced composite for bone implants. 2013: 17–26. Available from: https://www.doria.fi/bitstream/handle/10024/92662/Annales%20D%201087%20Nganga%20DISS.pdf?sequence=2

19. Ngaga S, Travan A, Marsich E, Donati I, Söderling E, Moritz N, et al. *In vitro* antimicrobial properties of silver-polysaccharide coatings on porous fiber-reinforced composites for bone implants. *J Mater Sci* 2013; **24**: 2775–85. doi: 10.1007/s10856-013-5022-2
20. He J, Söderling E, Lassila LV, Vallittu PK. Incorporation of an antibacterial and radiopaque monomer in to dental resin system. *Dent Mater* 2012; **28**: 110–17. doi: 10.1016/j.dental.2012.04.026
21. Atai M, Nekoomanesh M, Hashemi SA, Amani S. Physical and mechanical properties of an experimental dental composite based on a new monomer. *Dent Mater* 2004; **20**: 663–8.
22. Pereira SG, Osorio R, Toledano M, Nunes TG. Evaluation of two Bis-GMA analogues as potential monomer diluents to improve the mechanical properties of light-cured composite resins. *Dent Mater* 2005; **21**: 823–30.
23. Ruttermann S, Dluzhevskaya I, Grosssteinbeck C, Raab WH, Janda R. Impact of replacing Bis-GMA and TEGDMA by other commercially available monomers on the properties of resin-based composites. *Dent Mater* 2010; **26**: 353–9. doi: 10.1016/j.dental.2009.12.006
24. Vallittu PK, Miettinen V, Alakuijala P. Residual monomer content and its release into water from denture base materials. *Dent Mater* 1995; **11**: 338–42.
25. Chung CM, Kim MS, Kim JG, Jang DO. Synthesis and photopolymerization of trifunctional methacrylates and their application as dental monomers. *J Biomed Mater Res* 2002; **62**: 622–7.
26. Ge J, Trujillo M, Stansbury J. Synthesis and photopolymerization of low shrinkage methacrylate monomers containing bulky substituent groups. *Dent Mater* 2005; **21**: 1163–9.
27. Tuusa SM, Peltola MJ, Tirri T, Puska MA, Röyttä M, Aho H, et al. Reconstruction of critical size calvarial bone defects in rabbits with glass-fiber-reinforced composite with bioactive glass granule coating. *J Biomed Mater Res B Appl Biomater* 2008; **84**: 510–19.
28. Combe EC. Further studies on radio-opaque denture-base materials. *J Dent* 1972; **1**: 93–7.
29. Schulz H, Schimmoeller B, Pratsinis SE, Salz U, Bock T. Radiopaque dental adhesives: dispersion of flame-made Ta_2O_5/SiO_2 nanoparticles in methacrylic matrices. *J Dent* 2008; **36**: 579–87. doi: 10.1016/j.jdent.2008.04.010
30. Amirouche-Korichi A, Mouzali M, Watts DC. Effects of monomer ratios and highly radiopaque fillers on degree of conversion and shrinkage-strain of dental resin composites. *Dent Mater* 2009; **25**: 1411–18. doi: 10.1016/j.dental.2009.06.009
31. Schulze RK, Berndt D, d'Hoedt B. On cone-beam computed tomography artifacts induced by titanium implants. *Clin Oral Implants Res* 2010; **21**: 100–7. doi: 10.1111/j.1600-0501.2009.01817.x
32. Ludlow JB, Davis-Ludlow LE, Brooks SL, Howerton WB. Dosimetry of 3 CBCT devices for oral and maxillofacial radiology: CB Mercuray, NewTom 3G and i-Cat. *Dentomaxillofac Radiol* 2006; **35**: 219–26.
33. Ludllow JB, Ivanovic M. Comparative dosimetry of dental CBCT devices and 64-slice CT for oral and maxillofacial radiology. *Oral Surg Oral Med Oral Pathol Oral Radiol Endod* 2008; **106**: 930–8. doi: 10.1016/j.tripleo.2008.03.018
34. Pauwels R, Stamatakis H, Bosmans H, Bogaerts R, Jacobs R, Horner K, et al; The SEDENTEXCT Project Consortium. Quantification of metal artifacts on cone beam computed tomography images. *Clin Oral Implants Res* 2013; **24**: 94–9. doi: 10.1111/j.1600-0501.2011.02382.x
35. Chindasombatjareon J, Kakimoto N, Murakami S, Maeda Y, Furukawa S. Quantitative analysis of metallic artifacts caused by dental metals: comparison of cone-beam and multi-detector row CT scanners. *Oral Radiol* 2011; **27**: 114–20. doi: 10.1007/s11282-011-0071-z
36. Schulze D, Heiland M, Blake F, Rother U, Schmelzle R. Evaluation of quality of reformatted images from two cone-beam computed tomographic systems. *J Craniomaxillofac Surg* 2005; **33**: 19–23.
37. Hunter A, McDavid D. Analyzing the beam hardening artifact in the Planmeca Promax. *Oral Surg Oral Med Oral Pathol Oral Radiol Endod* 2009; **107**: 28–9.
38. Draenert FG, Coppenrath E, Herzog P, Müller S, Mueller-Lisse UG. Beam hardening artifacts occur in dental implant scans with the NewTom cone beam CT but not with the dental 4-row multidetector CT. *Dentomaxillofac Radiol* 2007; **36**: 198–203.
39. Scarfe WC, Farman AG. Cone-beam computed tomography. In: White SC, Pharoah MJ, ed. *Oral radiology: principles and interpretation*. St Louis, MO: Mosby; 2009. pp. 235–7.
40. Benic GI, Sancho-Puchades M, Jung RE, Deyhle H, Hämmerle C. *In vitro* assessment of artifacts induced by titanium dental implants in cone beam computed tomography. *Clin Oral Implants Res* 2013; **24**: 378–83. doi: 10.1111/clr.12048
41. Bryant JA, Drage NA, Richmond S. Study of the scan uniformity from an i-cat cone beam computed tomography dental imaging system. *Dentomaxillofac Radiol* 2008; **37**: 365–74. doi: 10.1259/dmfr/13227258